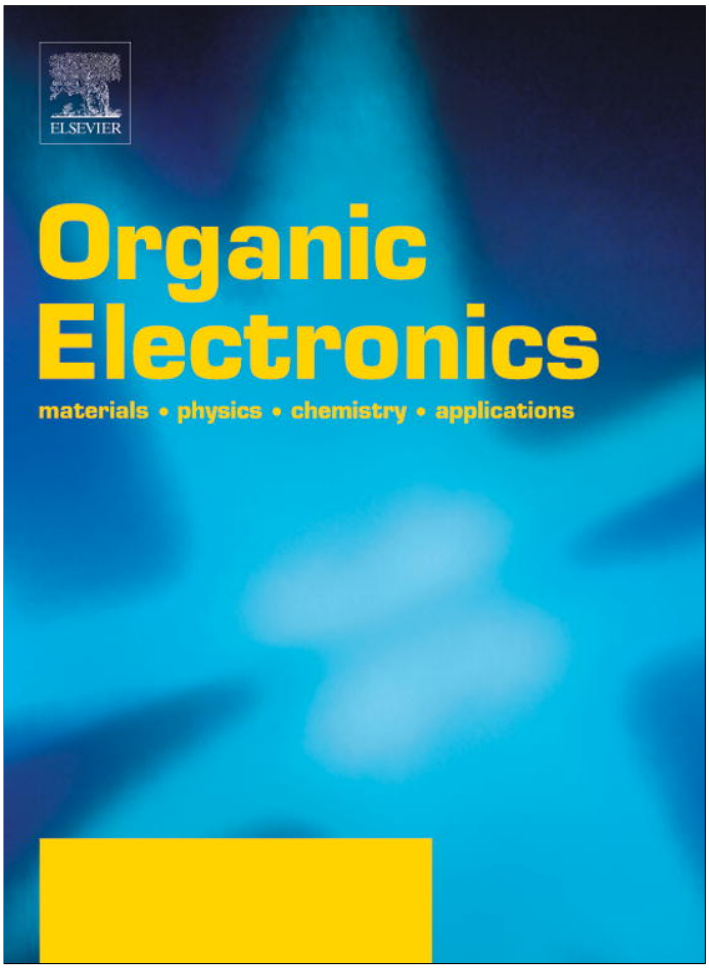

(This is a sample cover image for this issue. The actual cover is not yet available at this time.)

Organic Electronics 13 (2012) 2940–2944

Contents lists available at SciVerse ScienceDirect

Organic Electronics

journal homepage: www.elsevier.com/locate/orgel

Letter

All-spray-coated semitransparent inverted organic solar cells: From electron selective to anode layers

Jae-Wook Kang [a,*], Yong-Jin Kang [a,b], Sunghoon Jung [a], Dae Sung You [a], Myungkwan Song [a], Chang Su Kim [a], Do-Geun Kim [a], Jong-Kuk Kim [a], Soo H. Kim [b]

[a] Surface Technology Division, Korea Institute of Materials Science (KIMS), Changwon 641-831, Republic of Korea
[b] Department of Nanosystem and Nanoprocess Engineering, Pusan National University, Busan 609-735, Republic of Korea

ARTICLE INFO

Article history:
Received 4 March 2012
Received in revised form 7 August 2012
Accepted 7 August 2012
Available online 24 September 2012

Keywords:
All-spray coating
Semitransparent
Organic solar cell

ABSTRACT

We demonstrated an all-solution-processed electron selective layer, active layer and top electrode for large-area inverted organic solar cells. The fabricated devices are semitransparent, fully spray-coated, highly efficient and air-stable, with power efficiencies of 2.41% and 1.0% for cell areas of 0.36 and 15.25 cm^2, respectively. The shelf life of the cells in air is demonstrated by the ~80% retention of original cell efficiency after 30 days.

Development in the field of organic solar cells has been growing because of the large variety of low-cost production methods using an all-printing process on flexible substrates [1–9]. The all-printing process enables mass production of solar cells based on cost-effective roll-to-roll technologies [10,11]. For the all-printing process, an inverted architecture is usually used to avoid the vacuum process used for the deposition of the low-work-function metal electrodes (such as Al and Ca). A high work-function anode (such as Ag and Au) is used to collect holes, and an electron-selective layer on the surface of indium tin oxide (ITO) is used to collect electrons [12–14]. The all-spray-coating process is a very promising technique for fulfilling this requirement, owing to its simplicity and low-cost. One critical issue in this fabrication process is how to form a high-work-function top metal electrode using a solution process without damaging the device performance [11]. Although a few attempts to spray metal nanowires [15] and metal nanoparticles [16–17] as top metal electrode have been successful, our approach is to use the following layer sequence: transparent cathode/electron selective layer/active layer/poly(3,4-ethylene dioxythiophene doped with polystyrene sulfonate) (PEDOT:PSS) anode [9]. Further, to demonstrate semitransparent devices, the see-through transmittance can be adjusted by controlling the thickness of the active or PEDOT:PSS layers [18,19]. In this study, a spray-coating process is presented as a cost-effective large-area-printable process for semitransparent inverted organic solar cells (IOSCs) fabrication. The fabricated device is semitransparent, fully spray-coated, highly efficient and air-stable, with power efficiencies of 2.41% and 1.0% for cell areas of 0.36 and 15.25 cm^2, respectively, and ~80% retention of original efficiency after 30 days.

Fig. 1a illustrates the device fabrication process. All layers were coated by a spray-coating process in air atmosphere. Semitransparent IOSCs were fabricated on patterned ITO-coated glass substrates (sheet resistance ~4 ohm/sqr.) with 2.5 × 2.5 and 5.0 × 5.0 cm^2 sizes, which were first cleaned in an ultrasonic bath containing acetone and then boiled in isopropyl alcohol. The substrates were then dried in an oven and treated with UV–ozone for 5 min. The spray-coating system uses two nozzles as the

* Corresponding author. Tel.: +82 55 280 3572; fax: +82 55 280 3570.
E-mail address: jwkang@kims.re.kr (J.-W. Kang).

1566-1199/$ - see front matter © 2012 Elsevier B.V. All rights reserved.
http://dx.doi.org/10.1016/j.orgel.2012.08.012

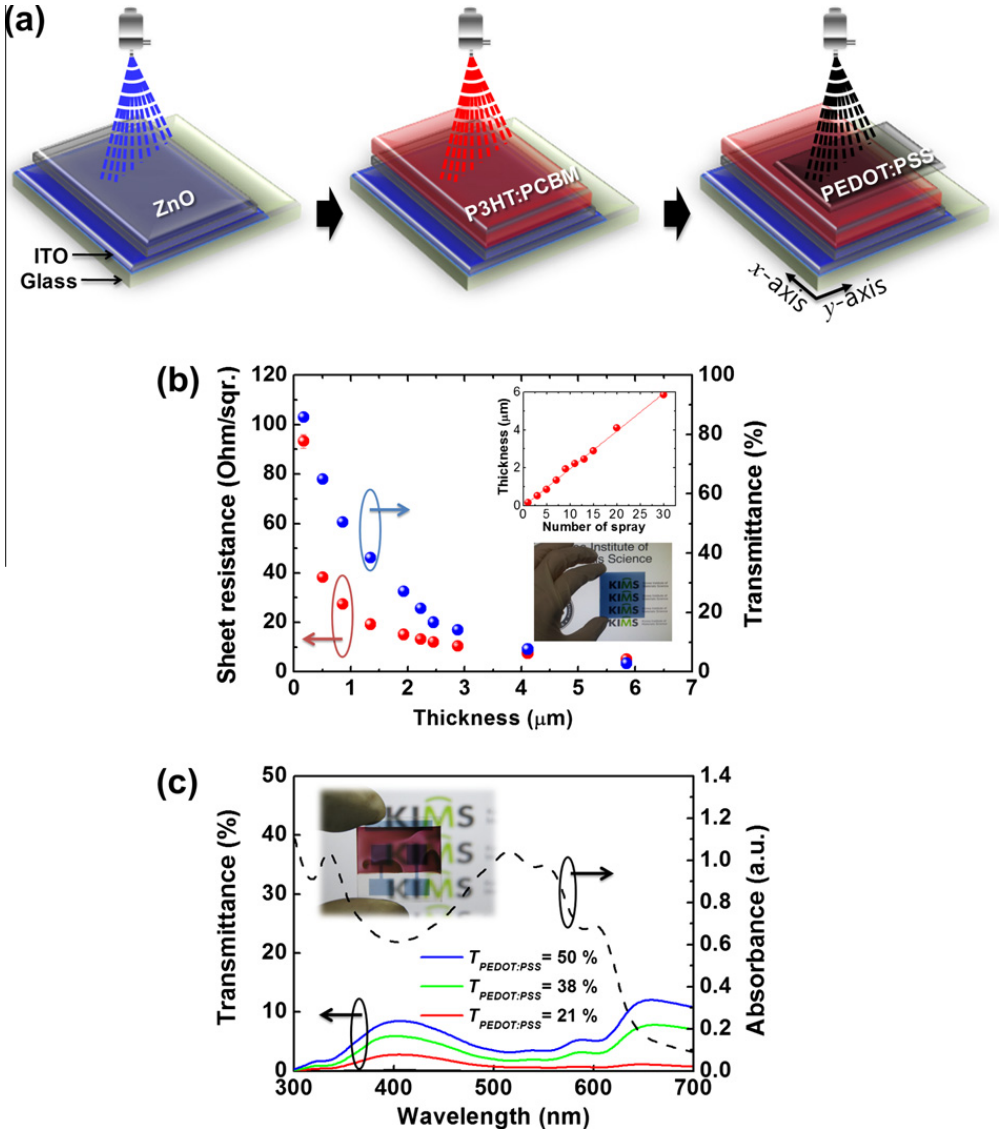

Fig. 1. (a) Schematic diagram of the all-spray coating process. (b) Sheet resistance and transmittance of 5 wt.% DMSO-doped PEDOT:PSS films as a function of thickness. The inset is the thickness of PEDOT:PSS films dependent on the number of spray coating and a photograph of 1-μm-thick PEDOT:PSS film. (c) Transmittance spectra of semitransparent IOSCs fabricated all-spray coating with different transmittance of PEDOT:PSS ($T_{PEDOT:PSS}$) anodes and absorbance spectrum of spray coated P3HT:PCBM thin film. The inset is a photograph of a semitransparent device with $T_{PEDOT:PSS}$ = 21%.

core and clad. The core nozzle was connected to an injection pump for the coating solution, and the clad nozzle was linked to compressed N_2 gas [21]. First, a thin film of zinc oxide (ZnO) was spray-coated onto the ITO glass substrate from a ZnO sol–gel solution and annealed at 300 °C for 20 min in air, resulting in a thickness of ~40 nm. Second, a poly (3-hexylthiophene):[6,6]-phehyl-C61 butyric acid methyl ester (P3HT:PCBM) blend solution prepared at 1:1 mass ratio in 1,2-dichlorobenzene (10 mg/ml P3HT and 10 mg/ml PCBM) was spray-coated onto the ZnO layer with a thickness of ~250 nm. Subsequently, for enhancements of charge carrier mobility and light absorption by increasing the crystallinity of P3HT, a solvent evaporation was performed for 2 h in a glove box at room temperature [22,23]. Finally, a PEDOT:PSS (PH 1000 from H.C. Starck) solution mixed with 5 wt.% of dimethyl sulfoxide (DMSO) was spray-coated onto the P3HT:PCBM layer with a substrate temperature of ~40 °C, because PEDOT:PSS cannot wet completely on active layer at 25 °C (Supporting Information Fig. S1). In the spray-coating of the PEDOT:PSS anode, a shadow mask was used to cover the active layer to form cell areas of either 0.36 cm^2 or 15.25 cm^2, and the films were annealed at 150 °C for 20 min in a glove box. The device performance for the spray-coated devices is affected by the thin film morphology resulting from varying the solvent, substrate temperature, solution injection rate, carrier gas flow, nozzle-substrate distance, and printing speed [22,24]. Detailed information of the optimized spray-coating conditions for ZnO and P3HT:PCBM layer can be found elsewhere [24]. In an opaque control device, the ~40-nm-thick ZnO, ~250-nm-thick P3HT:PCBM and ~40-nm-thick PEDOT:PSS (PH 1000) layers were all-spray coated. Finally, a 120-nm-thick Ag electrode was evaporated at 3×10^{-6} Torr. The fabricated IOSCs were characterized using restricted illumination by inserting a shadow mask to eliminate excess photocurrent from the conductive PEDOT:PSS layer [21,24]. The current–voltage (*J–V*) characteristics were measured under AM 1.5 simu-

lated illumination with an intensity of 100 mW/cm^2 (Pecell Technologies Inc., PEC-L11 model). The intensity of sunlight illumination was calibrated using a standard Si photodiode detector with a KG-5 filter. The *J–V* curves were recorded automatically with a Keithley SMU 2400 source meter by illuminating the IOSCs.

To increase PEDOT:PSS thickness for application in device electrodes, a multi-layer coating process was investigated to further lower the sheet resistance of the films, resulting in thickness that increased from 0.17 to 5.8 μm with number of spray coatings. Fig. 1b shows the behavior of transmittance and sheet resistance as a function of the thickness of the spray-coated 5 wt.% DMSO-doped PEDOT:PSS film. The electrical and optical properties of the PEDOT:PSS films depend distinctly on the film thickness [20]. The PEDOT:PSS films with thickness in the range of 0.85–5.8 μm exhibit promising sheet resistance and transmittance values in the ranges of 30–3 ohm/sqr. and 50–3%, respectively, showing that conductive polymers are an alternative to conventional metal as an anode electrode for IOSCs. The transparency of the all-spray-coated devices is shown in Fig. 1c, with a different transmittance for the PEDOT:PSS anodes ($T_{PEDOT:PSS}$). The inset is a picture of a semitransparent IOSC with $T_{PEDOT:PSS}$ = 21%. The transmittance of the IOSCs can be adjusted by controlling the thickness of the PEDOT:PSS layers. This semitransparent IOSC fabrication process has many advantages over regular methods. First of all, no vacuum process is involved, and three layers are coated by a cost-effective solution-based method. Second, this process is potentially easy to apply for large-area and roll-to-roll manufacturing processes. Third, the PEDOT:PSS anode in this device is very cost-effective and solution-processible [29], in contrast to the Ca [6–7,25], Ag, Au [14–17,18], or transparent oxide (ITO and zinc tin oxide) [26–28] anodes in regular devices, which are excessively reactive or expensive metals.

The effects of the transmittance of the PEDOT:PSS anode on the device characteristics of the all-spray-coated IOSCs have been studied. Fig. 2 shows the *J–V* characteristics of the semitransparent IOSCs illuminated from the glass side (bottom illumination) and the PEDOT:PSS side (top illumination). With a $T_{PEDOT:PSS}$ decreasing from 50% to 21%, the

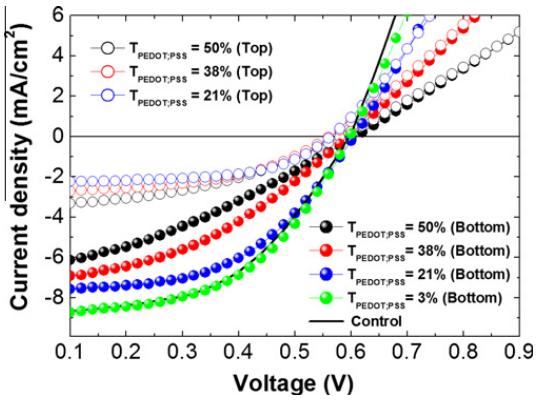

Fig. 2. Comparison of the photovoltaic response of all-spray-coated semitransparent IOSCs illuminated from the ITO glass side (bottom) and the PEDOT:PSS side (top) as a function of transmittance of PEDOT:PSS ($T_{PEDOT:PSS}$) anode. Control devices were opaque and fabricated with a structure of ITO/ZnO/P3HT:PCBM/PEDOT:PSS/Ag.

power conversion efficiency (PCE) of the semitransparent IOSC increased from 1.35% to 2.41% for the bottom illumination. The series resistance (R_s) of the IOSCs from the inverse slope of the *J–V* curve at *J* = 0 decreased significantly from 37.3 to 16.3 Ω cm^2 with increasing PEDOT:PSS thickness, resulting in an improvement of fill factor (*FF*) from 0.34 to 0.51. However, the top-illuminated devices showed PCEs that were slightly reduced from 0.83% to 0.74%, resulting from a greater reduction of J_{sc} than improvement of *FF*. Besides the solar cells with the semitransparent PEDOT:PSS anode, we investigated opaque control devices with a PEDOT:PSS(PH 1000)/Ag top electrode resulting in a PCE of 2.74 ± 0.1% (*FF* = 0.52 ± 0.04, R_s = 6 ± 0.5 Ω cm^2), which were comparable to the all-spray-coated IOSCs with a $T_{PEDOT:PSS}$ = 21% (PCE = 2.41%, *FF* = 0.51, R_s = 16.3 Ω cm^2). A summary of the respective electronic device properties is given in Table 1.

The all-spray coating process was also applied to fabricate large-area semitransparent IOSCs with a cell area of 15.25 cm^2 and a substrate size of 5.0 × 5.0 cm^2, as shown in Fig 3. By increasing the cell area from 0.36 to 15.25 cm^2, the PCE of the semitransparent IOSCs was reduced dramatically from 2.41% to 0.84%, resulting from the significant increase of R_s from 16.3 to 56 Ω cm^2. As the cell area increases up to 15.25 cm^2, the PCE drops significantly due to the drop of *FF* from 0.51 to 0.27 and the suppression of photocurrent from 7.74 to 5.19 mA cm^{-2}. The drop of *FF* and J_{sc} can be explained by the increase of R_s and the accelerating recombination of electrons and holes at low built-in-junction potential with increasing area, respectively [30]. In large-area applications, the spray-coated PEDOT:PSS anode has high series resistance, because the PEDOT:PSS thin film has lower conductivity than conventional metal. A simple way of decreasing the overall resistance of the PEDOT:PSS anode is to deposit thick metal grids using screen printing methods on top of the anode, which can provide an alternative, low-resistance pathway for the current [21,31–37]. The distance between the metal grids on top of the PEDOT:PSS anode is 1 mm, and the widths of an individual grid finger and busbar are 1 and 2 mm, respectively (Fig. 3c). The device with the metal grids showed better overall performance (J_{sc} = 5.80 mA cm^{-2}, *FF* = 0.29, R_s = 51.5 Ω cm^2 and PCE = 1.0%) than the large-area device without grids (J_{sc} = 5.19 mA cm^{-2}, *FF* = 0.27, R_s = 56.4 Ω cm^2 and PCE = 0.84%) resulting from

Table 1
The performance of the semitransparent IOSCs illuminated from top and bottom surfaces.

Illumination side	$T_{PEDOT:PSS}$[a] (%)	J_{sc} (mA cm^{-2})	V_{oc} (V)	*FF*	PCE (%)	R_s (Ω cm^2)
Top	50	3.47	0.581	0.41	0.83	35.2
Top	38	2.78	0.562	0.49	0.77	28.2
Top	21	2.28	0.563	0.58	0.74	12.1
Bottom	50	6.58	0.606	0.34	1.35	37.3
Bottom	38	7.21	0.594	0.40	1.75	29.4
Bottom	21	7.74	0.604	0.51	2.41	16.3
Bottom	3	8.18	0.595	0.52	2.53	13.6
Bottom[b]	–	8.91	0.597	0.52	2.74	6.12

[a] The transmittance of PEDOT:PSS film at 550 nm.
[b] Control device was opaque and fabricated with a structure of ITO/ZnO/P3HT:PCBM/PEDOT:PSS/Ag.

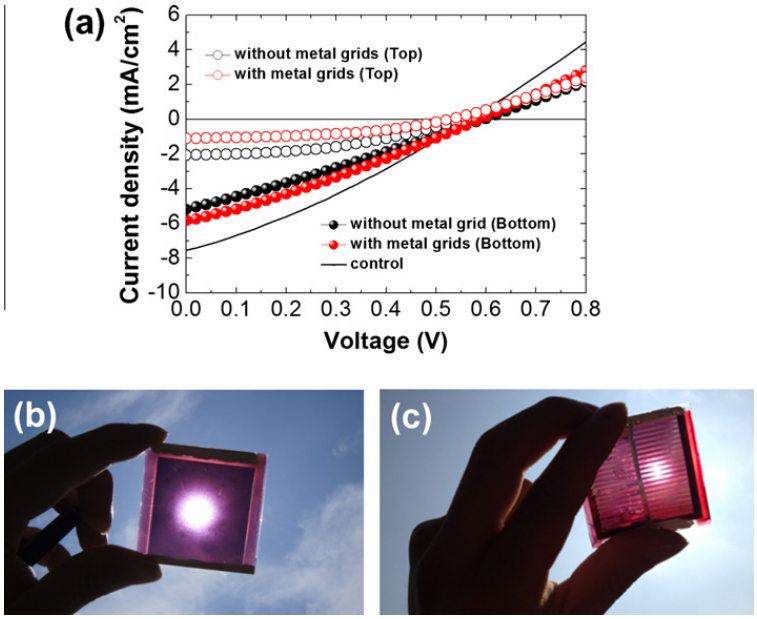

Fig. 3. (a) All-spray-coated large-area IOSCs in a cell area of 15.25 cm^2 using the $T_{PEDOT:PSS}$ = 21% with and without metal grids. Control device was opaque and fabricated with a structure of ITO/ZnO/P3HT:PCBM/PEDOT:PSS/Ag. The photographs of semitransparent large-area IOSCs with a PEDOT:PSS transmittance of 21%, (b) without and (c) with metal grids on top of PEDOT:PSS anode.

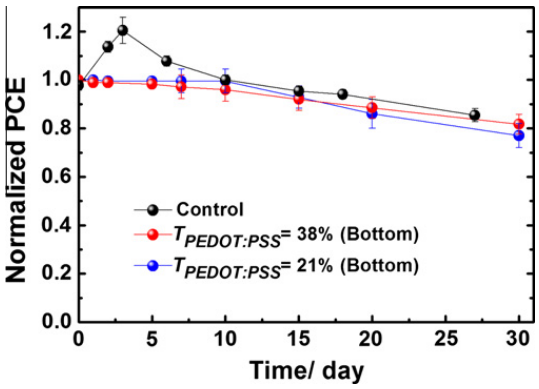

Fig. 4. Normalized PCE of the unencapsulated semitransparent and control IOSCs stored for 30 days in air under ambient conditions.

the decrease of R_s. Further, it shows device performance that is comparable to opaque large-area control devices with a PEDOT:PSS/Ag top electrode (PCE = 1.3 ± 0.1%). Fig. 4 shows the stability of the semitransparent IOSCs prepared by the all-spray-coating process. The stability studies were performed in the dark with ambient conditions tested according to the ISOS-D-1 (shelf) standard [30]. The performance of the semitransparent IOSCs was evaluated for 30 days. The normalized PCE of the unencapsulated semitransparent IOSCs after 30 days showed retention of ~80% of the original efficiency, which was similar to opaque control devices with a PEDOT:PSS/Ag top electrode.

In summary, an all-spray coating process was developed to take full advantage of the solution process for making cost-effective large-area printable semitransparent IOSCs. The preliminary results for semitransparent IOSCs show promising efficiency comparable to the regular opaque device, suggesting that this method will open a new direction for future low-cost organic-based electronic devices.

Acknowledgments

This study was supported by the New and Renewable Energy program of the Korea Institute of Energy Technology Evaluation and Planning (KETEP) (Grant Nos. 20113010010030 and 20103020010050) funded by the Ministry of the Knowledge Economy, Republic of Korea.

Appendix A. Supplementary material

Supplementary data associated with this article can be found, in the online version, at http://dx.doi.org/10.1016/j.orgel.2012.08.012.

References

[1] M. Manceau, D. Angmo, M. Jorgensen, F.C. Krebs, Org. Electron. 12 (2011) 566.
[2] J.Y. Kim, K. Lee, N.E. Coates, D. Moses, T.-Q. Nguyen, M. Dante, A.J. Heeger, Science 317 (2007) 222.
[3] G. Dennler, M.C. Scharber, C.J. Brabec, Adv. Mater. 21 (2009) 1323.
[4] J.E. Lewis, E. Lafalce, P. Toglia, X. Jiang, Sol. Energy Mater. Sol. Cells 95 (2011) 2816.
[5] M.M. Voigt, R.C.I. Mackenzie, C.P. Yau, P. Atienzar, J. Dane, P.E. Keivanidis, D.D.C. Bradley, J. Nelson, Sol. Energy Mater. Sol. Cells 95 (2010) 731.
[6] D. Vak, S.-S. Kim, J. Jo, S.-H. Oh, S.-I. Na, J. Kim, D.-Y. Kim, Appl. Phys. Lett. 91 (2007) 081102.
[7] R. Green, A. Morfa, A.J. Ferguson, N. Kopidakis, G. Rumbles, S.E. Shaheen, Appl. Phys. Lett. 92 (2008) 033301.
[8] C. Girotto, B.P. Rand, J. Genoe, P. Heremans, Sol. Energy Mater. Sol. Cells. 93 (2009) 454.
[9] Y.-F. Lim, S. Lee, D.J. Herman, M.T. Lloyd, J.E. Anthony, G.G. Malliaras, Appl. Phys. Lett. 93 (2008) 193301.
[10] C. Girotto, D. Moia, B.P. Rand, P. Heremans, Adv. Funct. Mater. 21 (2010) 64.
[11] S.-I. Na, B.-K. Yu, S.-S. Kim, D. Vak, T.-S. Kim, J.-S. Yeo, D.-Y. Kim, Sol. Energy Mater. Sol. Cells 93 (2010) 1333.
[12] W.H. Shim, S.-Y. Park, M.Y. Park, H.O. Seo, K.-D. Kim, Y.T. Kim, Y.D. Kim, J.-W. Kang, K.H. Lee, Y. Jeong, Y.D. Kim, D.C. Lim, Adv. Mater. 23 (2011) 519.

[13] S.K. Hau, H.-L. Yip, J. Zou, A.K.-Y. Jen, Org. Electron. 10 (2009) 1401.
[14] C.S. Kim, S.S. Lee, E.D. Gomez, J.B. Kim, Y.-L. Loo, Appl. Phys. Lett. 94 (2009) 113302.
[15] W. Gaynor, J.-Y. Lee, P. Peumans, Nano Lett. 4 (2010) 30.
[16] C. Girotto, B.P. Rand, S. Steudel, J. Genoe, P. Heremans, Org. Electron. 10 (2009) 735.
[17] S.K. Hau, H.-L. Yip, K. Leong, A.K.-Y. Jen, Org. Electron. 10 (2009) 719.
[18] T. Ameri, G. Dennler, C. Waldauf, H. Azimi, A. Seemann, K. Forberich, J. Hauch, M. Scharber, K. Hingerl, C.J. Brabec, Adv. Funct. Mater. 20 (2010) 1592.
[19] Y. Zhou, H. Cheun, S. Choi, C. Fuentes-Hernandez, B. Kippelen, Org. Electron. 12 (2011) 827.
[20] Y.H. Kim, C. Sachse, M.L. Machala, C. May, L. Muller-Meskamp, K. Leo, Adv. Funct. Mater. 21 (2011) 1076.
[21] S.-Y. Park, Y.-J. Kang, S. Lee, D.-G. Kim, J.-K. Kim, J.-H. Kim, J.-W. Kang, Sol. Energy Mater. Sol. Cells 95 (2011) 852.
[22] G. Susanna, L. Salamandra, T.M. Brown, A.D. Carlo, F. Brunetti, A. Reale, Sol. Energy Mater. Sol. Cells 95 (2011) 1775.
[23] G. Li, V. Shrotriya, J. Huang, Y. Yao, T. Moriarty, K. Emery, Y. Yang, Nature Mater. 4 (2005) 864.
[24] J.W. Kang, Y.-J. Kang, S. Jung, M. Song, D.-G. Kim, C.-S. Kim, S.H. Kim, Sol. Energy Mater. Sol. Cells. 103 (2012) 76.
[25] G.-M. Ng, E.L. Kietzke, T. Kietzke, L.-W. Tan, P.-K. Liew, F. Zhu, Appl. Phys. Lett. 90 (2007) 103505.
[26] H. Schmidt, H. Flugge, T. Winkler, T. Bulow, T. Riedl, W. Kowalsky, Appl. Phys. Lett. 94 (2009) 243302.
[27] T. Winkler, H. Schmidt, H. Flugge, F. Nikolayzik, I. Barmann, S. Schmale, T. Weimann, P. Hinze, H.-H. Johannes, T. Rabe, S. Hamwi, T. Riedl, W. Kowalsky, Org. Electron. 12 (2011) 1618.
[28] J. Huang, G. Li, Y. Yang, Adv. Mater. 20 (2008) 415.
[29] C.J.M. Emmott, A. Urbina, J. Nelson, Sol. Energy Mater. Sol. Cells 97 (2012) 14.
[30] M.O. Reese, S.A. Gevorgyan, M. Jørgensen, E. Bundgaard, S.R. Kurtz, D.S. Ginley, D.C. Olson, M.T. Lloyd, P. Morvillo, E.A. Katz, A. Elschner, O. Haillant, T.R. Currier, V. Shrotriya, M. Hermenau, M. Riede, K.R. Kirov, G. Trimmel, T. Rath, O. Inganas, F. Zhang, M. Andersson, K. Tvingstedt, M. Lira-Cantu, D. Laird, C. McGuiness, S.J. Gowrisanker, M. Pannone, M. Xiao, J. Hauch, R. Steim, D.M. DeLongchamp, Roland Rösch, H. Hoppe, N. Espinosa, A. Urbina, G. Yaman-Uzunoglu, J.-B. Bonekamp, A.J.J.M. van Breemen, C. Girotto, E. Voroshazi, F.C. Krebs, Sol. Energy Mater. Sol. Cells 95 (2011) 1253.
[31] W.-I. Jeong, J. Lee, S.-Y. Park, J.-W. Kang, J.-J. Kim, Adv. Funct. Mater. 21 (2011) 343.
[32] S.-Y. Park, W.-I. Jeong, D.-G. Kim, J.-K. Kim, D.C. Lim, J.H. Kim, J.-J. Kim, J.-W. Kang, Appl. Phys. Lett. 96 (2010) 173301.
[33] K. Tvingstedt, O. Inganas, Adv. Mater 19 (2007) 2893.
[34] J. Zou, H.-L. Yip, S.K. Hau, A.K.Y. Jen, Appl. Phys. Lett 96 (2010) 203301.
[35] T. Aernouts, P. Vanlaeke, W. Geens, J. Poortmans, P. Heremans, S. Borghs, R. Mertens, R. Andriessen, L. Leenders, Thin Solid Films 451–452 (2004) 22.
[36] F.C. Krebs, Sol. Energy Mater. Sol. Cells 93 (2009) 394.
[37] Y. Galagan, B. Zimmermann, E.W.C. Coenen, M. Jørgensen, D.M. Tanenbaum, F.C. Krebs, H. Gorter, S. Sabik, L.H. Slooff, S.C. Veenstra, J.M. Kroon, R. Andriessen, Adv. Energy Mater 2 (2012) 103.